Published in final edited form as:
Virology. 2014 January 20; 449: 163–173. doi:10.1016/j.virol.2013.10.035.

Biodistribution, pharmacokinetics, and blood compatibility of native and PEGylated tobacco mosaic virus nano-rods and -spheres in mice

Michael A. Bruckman[1], **Lauren N. Randolph**[1], **Allen VanMeter**[1], **Stephen Hern**[1], **Andrew J. Shoffstall**[1], **Rebecca E. Taurog**[5], and **Nicole F. Steinmetz**[*,1,2,3,4]

[1]Department of Biomedical Engineering, Case Western Reserve University, 10900 Euclid Ave., Cleveland, OH 44106, USA

[2]Department of Radiology, Case Western Reserve University, 10900 Euclid Ave., Cleveland, OH 44106, USA

[3]Department of Materials Science and Engineering, Case Western Reserve University, 10900 Euclid Ave., Cleveland, OH 44106, USA

[4]Department of Macromolecular Science and Engineering, Case Western Reserve University, 10900 Euclid Ave., Cleveland, OH 44106, USA

[5]Department of Chemistry, Williams College, 47 Lab Campus Drive, Williamstown, MA 01267, USA

Abstract

Understanding the pharmacokinetics, blood compatibility, biodistribution and clearance properties of nanoparticles is of great importance to their translation to clinical application. In this paper we report the biodistribution and pharmacokinetic properties of tobacco mosaic virus (TMV) in the forms of 300×18 nm rods and 54 nm-sized spheres. The availability of rods and spheres made of the same protein provides a unique scaffold to study the effect of nanoparticle shape on *in vivo* fate. For enhanced biocompatibility, we also considered a PEGylated formulation. Overall, the versions of nanoparticles exhibited comparable *in vivo* profiles; a few differences were noted: data indicate that rods circulate longer than spheres, illustrating the effect that shape plays on circulation. Also, PEGylation increased circulation times. We found that macrophages in the liver and spleen cleared the TMV rods and spheres from circulation. In the spleen, the viral nanoparticles trafficked through the marginal zone before eventually co-localizing in B-cell follicles. TMV rods and spheres were cleared from the liver and spleen within days with no apparent changes in histology, it was noted that spheres are more rapidly cleared from tissues compared to rods. Further, blood biocompatibility was supported, as none of the formulations induced clotting or hemolysis. This work lays the foundation for further application and tailoring of TMV for biomedical applications.

[*]Corresponding author: Prof. Nicole F. Steinmetz, Department of Biomedical Engineering, Radiology, Materials Science and Engineering, Macromolecular Science and Engineering, Case Western Reserve University, Schools of Medicine and Engineering, 10900 Euclid Avenue, Cleveland, OH 44106, USA, phone: 216-844-8164, nicole.steinmetz@case.edu.

Keywords

viral nanoparticle; tobacco mosaic virus; PEGylation; nanoparticle shape; biodistribution; blood compatibility; pharmacokinetics

Introduction

Nanoparticles hold great potential for clinical research and application for diagnosing and treating diseases [1]. Nanoparticles are used to deliver a high payload of cargo, such as imaging and therapeutic compounds, to specific sites of disease while avoiding healthy tissue. While receptor-specific ligands can direct these nanoparticles to target specific cells and tissues, a majority of the injected dose is cleared by the reticuloendothelial system (RES) and mononuclear phagocyte system (MPS) [2]. On the road toward clinical translation of any nanoparticle platform, a detailed understanding of the body's response to the nanoparticles is required; this will allow tailoring and optimizing biodistribution and clearance.

Viral nanoparticles (VNPs) are protein-based, nanoscale materials designed by nature to deliver cargos to cells; being natural experts at cargo delivery led to their study and application as drug and contrast agent delivery vehicles. There are a number of reasons that make VNPs excellent platforms for applications in biomedicine, including their biocompatibility, biodegradability, high monodispersity, and ease of production and functionalization. Platform simplicity and high processability are key components for clinical translation of nanoparticle platforms – VNPs offer this through their genetic engineering capabilities and simple purification protocols. A library of VNPs is available and currently under investigation for clinical applications. These include the plant viruses cowpea mosaic virus (CPMV) and potato virus X (PVX), as well as bacteriophages such as M13 and P22 [3]. For example, it has been demonstrated that 30 nm-sized icosahdral CPMV target tumor cells and the inflamed endothelium in atherosclerotic plaques, based on its natural interactions with cell surface expressed vimentin [4, 5]. Also, targeting ligands specific to the vascular endothelial growth factor receptor-1 or gastrin-releasing peptide receptors have been used to re-direct CPMV to tumor endothelial cells and cancer cells in preclinical mouse models [4, 6]. Recent data indicate that in addition to tailoring the VNP surface chemistry [7], VNP shape can also be used as a handle to tailor biodistribution and tissue penetration properties [8-10]. For example, we showed that filamentous PVX has enhanced passive tumor homing and deeper tissue penetration compared to icosahedral CPMV nanoparticles. While both platforms were cleared by MPS and accumulated in liver and spleen, differences were noted: PVX was mostly retained in the spleen, and CPMV in the liver [11]. However, it should be noted that besides the shape-derived differences, PVX and CPMV also differ in their protein make up. Therefore, in this work, we turned toward the evaluation of biodistribution and clearance of VNP-based materials of identical protein make up but different shape, specifically the rods and spheres, of tobacco mosaic virus (TMV).

TMV is a rod-shaped VNP measuring 300 nm in length, 18 nm in diameter and a 4 nm-wide interior channel; its structure is known to atomic resolution [12]. This stiff rod-shaped nanoparticle has been utilized as a material for a variety of applications in nanotechnology [13, 14]. Chemically and genetically engineered TMV particles have being developed and tested for applications as light harvesting systems [15, 16], energy storage [17], sensing [18], cell growth [19, 20], magnetic resonance imaging contrast enhancement [21], and vaccine development [22-25]. Recently Atabekov et al. have shown that TMV can undergo thermal transition to form RNA-free spherical nanoparticles (SNPs) [26]. The thermal denaturation

of TMV rods yields insoluble coat proteins that somewhat surprisingly associate with each other to assemble into highly stable SNPs. The size of the TMV SNPs can be tightly tuned through adjustment of the protein concentration: at higher concentration (10 mg/mL), up to 800 nm-sized SNPs are formed, and at lower concentrations (0.1 mg/mL), SNPs as small as 50 nm are formed [26]. Further, it was shown that SNPs can be coated with a variety of polymers and proteins [27]. Following electrostatic binding, formaldehyde can bond the proteins to the SNP surface. Protein-functionalized SNPs are under development for vaccines [28].

To us, the TMV rods and SNPs provide a interesting platform to investigate the impact of shape on biodistribution and clearance. We would like to acknowledge that the TMV rods and spheres are not identical in their structural properties: while the TMV rod consists of a helical arrangement of precisely arranged coat proteins, the SNPs consist of aggregated, most likely denatured, coat proteins. Nevertheless, the TMV rods and SNPs are made up of the same proteins and zeta potential measurements support that the rods and spheres have comparable surface charge (see results). Therefore, we reasoned, that the TMV rod and SNP platform would be suitable tools for investigation of their *in vivo* properties. This is also important considering that several groups have turned toward the development of the platforms for potential applications in medicine and materials (see above).

Here, we report the study of TMV and SNP biodistribution, clearance, and blood compatibility in mice. The application of rods and spheres allow us to provide further insights into the impact of shape on the *in vivo* fate of nanoparticles. Further, we investigated the effect of PEGylation: native and PEGylated TMV rods were studied. PEG was applied because of its known properties to enhance solubility and biocompatibility of intravenously administered nanoparticles [29].

Materials/Methods

Isolation of TMV

TMV was produced in *Nicotiana benthamiana* plants; 6-8 weeks after seeding, plants were infected through mechanical inoculation. Infected leaves were harvested 14-21 days after infection and stored at −80°C. TMV was extracted in yields of 4.5 mg per gram of infected leaf material using established methods [30]. TMV concentration was determined using UV-Vis absorbance (ε at 260 nm = 3.0 mg^{-1} mL cm^{-1}), and virus particle structural integrity was confirmed using transmission electron microscopy (TEM) and size exclusion chromatography (SEC) (see below).

Synthesis of Cy5-TMV and PEG-Cy5-TMV

All reagents were purchased from Fisher Scientific unless otherwise specified. The following protocols were modified from established methods [21]. Briefly, TMV was decorated with terminal alkynes at external Tyr side chains by reaction with an *in situ* generated diazonium salt (3-ethynylaniline mixed with sodium nitrite in an acidic solution). Next, TMV rods underwent a copper-catalyzed azide-alkyne cycloaddition (CuAAC) reaction by reacting either 2 molar equivalents of sulfo-Cy5-azide (Lumiprobe) for Cy5-TMV or 2 molar equivalents of sulf-Cy5-azide and 2 molar equivalents of azide-$mPEG_{2000}$ (Nanocs Inc.) for PEG-Cy5-TMV with the exterior alkyne TMV (eAlk-TMV). Reactions were performed in 10 mM phosphate buffer at pH 7.0 with TMV (2 mg/mL), copper sulfate (1 mM), sodium ascorbate (2 mM), and aminoguanidine (2 mM) for 30 minutes on ice. The reaction mix was purified using a 10-40% sucrose gradient (made using a Biocomp Instruments Gradient Master) and ultracentrifugation and analyzed by TEM, SEC, and MALDI-TOF MS (see below).

Synthesis of Cy5-SNP

Fluorescent SNPs were produced by first labeling TMV rods with Cy5 dyes on their interior channel followed by thermal transitioning to SNPs. Interior Cy5 labeling was adapted from a previously reported protocol [21]. Briefly, to a solution of TMV (2 mg/mL) in 100 mM HEPES buffer pH 7.4, propargyl amine (2.7 mM), ethyldimethylaminopropylcarbodiimide (4.8 mM), and n-hydroxybenzotriazole (4.8 mM) was added to label interior Glu acid residues; the reaction was incubated for 24 hours at room temperature. The reaction was purified by sucrose cushion ultracentrifugation. Next, the interior alkynes underwent CuAAC reaction with sulfo-Cy5-azide (2 molar equivalents) using the procedure stated above. SNPs were generated trough heat transformation using a solution of 0.05 mg/mL TMV containing 0.5% PEG (w/v) in distilled H_2O. SNPs were formed using a PCR thermocycler with the following program: 4°C for 5 minutes, 96°C for 15 seconds, 4°C for 10 minutes. SNPs were then concentrated using spin filter concentrators. SNP protein concentration was determined by SDS-PAGE lane analysis (ImageJ) and UV-Vis absorbance at 260 nm. The size and morphology of SNPs were confirmed by TEM, SEM, and dynamic light scattering (DLS).

Transmission and scanning electron microscopy (TEM and SEM)

For TEM, formvar carbon film coated copper TEM grids (Electron Microscopy Sciences) were floated on drops of TMV rods or SNPs (20 μL, 0.1 mg/mL) for 2 minutes, washed with DI water, and negatively stained with 2% (w/v) uranyl acetate in DI water for 2 minute. Samples were examined using a Zeiss Libra 200FE transmission electron microscope operated at 200 kV. For SEM, samples were dried onto 5×5 mm silicon wafers (Ted Pella, Inc.) and then mounted on the surface of an aluminium pin stub with use of double-sided adhesive carbon discs (Agar Scientific). The stubs were then sputter-coated with gold in a high-resolution sputter coater (Agar Scientific, Ltd.) and transferred to a Hitachi 4500 scanning electron microscope operated at 5 kV.

Size exclusion chromatography (SEC)

All particles were analyzed by SEC using a Superose6 column on the ÄKTA Explorer chromatography system (GE Healthcare). Samples (100 μL, 1.0 mg/ml) were analyzed at absorbance wavelengths of 260, 280, 647 nm at a flow rate of 0.5 mL/min using 0.1 M potassium phosphate buffer pH 7.0.

Zeta potential analysis

The zeta potential for each sample was determined by placing a 0.01 mg/ml solution of sample in a 90Plus particle size analyzer (Brookhaven Instruments Corporation).

MALDI-TOF MS analysis

For MALDI-TOF MS analysis, native and modified TMV were denatured by adding 6 μL guanidine hydrochloride (6 M) to 24 μL sample (<1 mg/ml) in DI water and mixing for 5 minutes at room temperature. Denatured proteins were spotted on MTP 384 massive target plate using Zip-$Tips_{\mu C18}$ (Millipore). MALDI-TOF MS analysis was performed using a Bruker Ultra-Flex I TOF/TOF mass spectrometer.

Gel electrophoresis

Denaturing gel electrophoresis was used to analyze protein subunits, specifically proteins were analyzed on denaturing 4-12% NuPAGE gels (Invitrogen) using 1× MOPS running buffer (Invitrogen) and 10 μg of sample. After separation, the gel was photographed using an AlphaImager (Biosciences) imaging system after staining with Coomassie Blue. ImageJ

software (rsbweb.nih.gov/ij/, Supporting Information) was used for band analysis and to determine the protein concentration per SNP.

Animals

All experiments were carried out in accordance to the Case Western Reserve University's Institutional Animal Care and Use Committee. Female Balb/c mice were used for all experiments. Ten to fourteen-week old animals were used for all studies, and mice were maintained on an alfalfa-free diet (Teklad) for at least two weeks prior to viral nanoparticle administration via tail vein injection.

Pharmacokinetics studies

Modified TMV and SNPs were administered intravenously via the tail vein at a dosage of 10 mg/kg body weight. Blood was collected by orbital sinus bleeds and cardiac puncture. Blood samples were collected at 3, 5, 10, 15, 20, 30, 40, 60, 80, 100, 200, 400, and 1400 minutes (n=3 for each time point). The samples were centrifuged for 15 minutes at 7,000 rpm in a tabletop centrifuge to remove blood cells from plasma. The plasma was analyzed using a fluorescence plate reader (λ_{Ex} 600 nm and λ_{Em} 665 nm). Data were analyzed using Prism software.

Hemolysis assay

Blood was collected and pooled from three Balb/c mice. Within one hour of collection, pooled blood was centrifuged at 500 × g for 10 minutes, the supernatant was removed and calcium/magnesium-free DPBS (HyClone) was added to reach previous volume. Centrifugation was repeated two more times at 1,000 × g for 10 minutes. The red blood cells (RBCs) were counted and diluted to 1×10^9 cells/mL in Ca/Mg free DPBS. Twenty μL of RBCs were mixed with 20 μL sample and incubated in 37°C water bath for 1 hour. Samples tested: (PEGylated) TMV and SNP (5 mg/ml), DPBS was used for a negative control, and 1% (v/v) Triton X-100 was used as a positive control. The solutions were centrifuged for 10 minutes at 1,000 × g to remove intact RBCs. The absorbance of the resulting supernatant was tested at 540 nm for hemoglobin content on a Thermo Scientific NanoDrop 2000 Spectrophotometer. Percent hemolysis was calculated by dividing the sample absorbance by the absorbance achieved with 1% Triton X-100.

Coagulation Assay

Coagulation assays were performed in citrated whole blood (3.8% sodium citrate; 1:9 ratio; obtained via cardiac puncture from anesthetized Sprague Dawley rats). Thromboelastometry measurements were run using a Gamma ROTEM (Rotem Inc., Durham, NC), using the company's non-activated (NATEM) test in the presence of either saline or the viral nanoparticles (5 mg/ml). The outcomes considered included the standard ROTEM parameters clotting time (CT), clot formation time (CFT), the sum of the two (CT+CFT), and maximum clot firmness (MCF). CT is defined as the time from the start of the assay until the initial clotting is detected (thickness = 2 mm). CFT is defined as the time between clot initiation until a clot thickness of 20 mm is detected. MCF is defined as the maximum thickness (in mm) that a clot reaches during the duration of the test [31]. The study was performed using blood samples from 3 rats and each sample was normalized to a saline control. Statistical analysis was performed using a one-way ANOVA of the raw data (not normalized), with a Dunnett's comparison test between treatment groups and the saline control.

Biodistribution analysis

Ten to fourteen week old Balb/c mice were injected with a dose of 10 mg/kg modified TMV/SNP via the tail vein. The mice were sacrificed at 4, 24, and 96 hours, perfused with PBS, and the heart, brain, lung, spleen, liver, kidneys, and stomach, were collected (*n*=3 animals for each time point). The organs were cut in half and one half placed in a tube and plunged in liquid nitrogen and stored at −80°C. The frozen organs were thawed and mixed with PBS (100 mg organ per mL PBS). They were then homogenized and centrifuged at 7,500 × g for 10 minutes, 2 times to remove tissue debris; the supernatant was measured for fluorescence intensity using a fluorescence plate reader (λ_{Ex} 600 nm and λ_{Em} 665 nm). The second half of the organs was embedded in OCT media for cryosectioning and immunohistochemistry and –fluorescence studies (see below).

Immunohistochemistry and -fluorescence

Embedded organs were sectioned at 10 μm using a Leica CM 1850 cryostat. The frozen sections were then fixed with 95% ethanol for 10 minutes at −20°C, blocked with 10% (v/v) goat serum in DPBS for one hour at room temperature. After washing with DPBS, the primary antibody was bound for one hour at room temperature in 1% (v/v) goat serum in DPBS. The primary antibodies used here were F4/80 (Biolegend, stains macrophages), FITC-B220 (Biolegend, stains B-Cells), and CD3 (Biolegend, stains T-Cells); 250:1 dilutions were used for all antibodies. The F4/80 and CD3 antibodies required a secondary antibody for fluorescence imaging, Alexa Fluor 488 or 555-labeled secondary antibodies (Invitrogen) were used, 250:1 dilutions were used. Finally, cell nuclei were stained using DAPI (Sigma) diluted 9,500:1 for 20 minutes. Slides were mounted and analyzed using a Fluoview FV1000 (Olympus) confocal microscope.

H&E histology

Embedded organs were sectioned at 10 μm using a Leica CM 1850 cryostat. The frozen sections were fixed with 95% ethanol for 5 minutes at −20°C then air-dried. After washing with DI water, the slides were stained with hematoxylin (Richard-Allen Scientific) for 45 seconds. The tissues were washed with 70%, 80%, and 100% ethanol for three minutes each, sequentially, then stained with eosin for one minute. The tissues were mounted and analyzed with a Zeiss Observer.Z1 inverted microscope.

Results

Properties of TMV-based nanorods and nanoparticles Cy5-TMV, PEG-Cy5-TMV, and Cy5-SNP

TMV was produced at yields of 4.5 mg pure TMV per 1 g infected plant material using a one-day purification protocol [30]. Three different TMV-based nanoparticle formulations were produced for evaluation of biodistribution, pharmacokinetics, and blood compatibility in mice. Previously established bioconjugation and thermal transition protocols were used to produce dye-labeled TMV rods (Cy5-TMV), PEG_{2000}-coated dye-labeled TMV rods (PEG-Cy5-TMV), and dye-labeled TMV spheres (Cy5-SNPs) (Figure 1) [21]. In brief, TMV rods were labeled with Cy5 (and PEG_{2000}) at exterior tyrosine residues (TYR139) using a two-step diazonium coupling and CuAAC reaction protocol. Dye-labeled SNPs were obtained by heating interior Cy5-labeled TMV particles for 15 seconds at 96°C [21]. Interior labeling of the TMV rod is accomplished by labeling GLU97 and GLU106 with an alkyne handle followed by CuAAC chemistry protocols to introduce the fluorophores. (Bioconjugation methods for modification of SNPs are currently under development in our laboratory, however, not yet fully implemented. Therefore it was not possible to study PEGylated SNPs.)

The resulting Cy5-labeled (and PEGylated) TMV rods and SNPs were characterized for labeling efficiency, size, morphology, and surface properties using a combination of TEM and SEM, DLS, UV-Vis absorbance, SDS-PAGE, SEC, zeta potential, and MALDI-TOF MS. UV-Vis absorbance confirmed the attachment of about 900 Cy5 dyes per Cy5-TMV and PEG-Cy-TMV; this equates to a labeling efficiency of ~ 50%, meaning that every second Tyr residue was modified with a Cy5 dye (a single 300 nm-long TMV rod is comprised of 2130 identical copies of one coat protein). About 600 Cy5 dyes were conjugated to SNPs, meaning that 15% of the 4,260 interior glutamic acids per TMV were modified. The lower labeling efficiency may be explained by steric hindrance and lower accessibility of the interior *versus* exterior surface. Based on MALDI-TOF MS and SDS-PAGE lane analysis (Figure 2), we estimated coverage of PEG-Cy5-TMV with approximately 400 PEG_{2000} chains/TMV, which equates to a labeling efficiency of 20%.

TEM (Figure 2) and SEM images (not shown) confirmed the structural integrity of the particle formulations. It should be noted that based on the length of the RNA-genome, fully-assembled TMV nanorods have a length of 300 nm (and a width of 18 nm with a 4 nm-wide interior channel). A distribution of lengths is observed in TEM imaging, which could be explained by the fact that intermediate states as well as broken TMV rods are observed in TEM imaging. SNPs were measured at 54±14 nm based on TEM and 83±6 nm based on DLS (Figure 2). Based on the measured protein concentration and SNP size observed, we estimate that each SNP is formed by a single TMV rod. This is also in good agreement with the volume of a TMV cylinder and sphere composed of the same number of proteins.

Finally, the zeta potential of Cy5-TMV, PEG-Cy5-TMV, and Cy5-SNP was determined at −18, −17, −10 mV, respectively (Figure 2). The slightly lower zeta potential for SNPs is attributed to the loss of RNA following thermal transition.

Pharmacokinetics of TMV rods and SNPs differs

Plasma circulation half-life was determined in healthy Balb/c mice after intravenous bolus injection of 10 mg/kg Cy5-labeled (and PEGylated) TMV/SNP formulation (Figure 3). Plasma spiked with known TMV and SNP concentrations was measured to establish a standard curve, which was used to determine the percent-injected dose (%ID) in circulation. For pharmacokinetic analysis of nanoparticles, the following mathematical models are most commonly used: *non-compartmental* in which the area under the curve is considered, *compartmentalized one-phase* in which one considers the body as one blood pool with no organs, and *compartmentalized two-phase* in which one considers a quick circulating blood pool and slower blood flow in organs. We analyzed and fitted our data for these models and found that the TMV and SNP pharmacokinetics best fit according to the compartmentalized two-phase clearance mechanism. The first phase is characterized by a quick clearance, achieved through tissue distribution (liver and spleen), referred to as the distribution or equilibrium phase. The longer second phase involves a more active metabolic clearance mechanism and is referred to as the elimination phase. The phase I half-life for Cy5-TMV, PEG-Cy5-TMV, and Cy5-SNP were calculated at 3.5, 6.3, and 2.3 minutes, respectively, phase II values were 94.9, 44.4, and 58.2 minutes, respectively. Data indicate that PEGylation of TMV rods doubles the phase I half-life. Furthermore, shape appears to have a significant impact: the percent-injected dose of elongated Cy5-TMV and Cy5-PEG-TMV rods remaining in circulation is significantly higher compared to the amount of Cy5-SNPs remaining in circulation (~ 20% ID TMV rods *versus* 5% ID SNP Figure 3, inset).

Blood biocompatibility: TMV and SNP formulations do not induce hemolysis or blood clotting

The blood compatibility of TMV rods and SNPs was tested utilizing two general assays: red blood cell (RBC) disruption (hemolysis) and blood coagulation. Hemolysis was measured by incubating purified RBCs with TMV/SNP formulations. The incubation ratio of 2.5 mg/mL TMV to 5×10^8 RBCs/mL represents a roughly 1,000× higher ratio of nanoparticles to RBCs compared to the injected dose used for *in vivo* studies (mouse blood contains ~10×10^9 RBCs/mL). Following a one-hour incubation, RBCs were pelleted and the hemoglobin content – which is released after RBC lysis – was measured by reading the absorbance at 540 nm (Figure 4A and B). Data indicate that none of the formulations tested induced hemolysis.

Next, the effect of TMV/SNP formulations on blood clotting parameters was measured using rotational thromboelastometry. The ROTEM test utilized a whole-blood sample, with no platelet or coagulation activating agents added. In the present study, mean changes in the sum of clotting time and clot formation time (CT+CFT) and the maximum clot firmness (MCF) in the presence of TMV/SNP formulations differed no more than 5% from the saline baseline, suggesting a negligible impact of the nanoparticles on the coagulation mechanism (Figure 4C and D).

Biodistribution and clearance: SNPs and TMV show broad organ distribution, but SNPs show faster tissue clearance

The organ biodistribution for Cy5-TMV, Cy5-PEG-TMV, and Cy5-SNP was determined after intravenous tail vein injection of 10 mg/kg TMV/SNP and subsequent sacrifice of healthy Balb/c mice at 4, 24, and 96 hours. Following perfusion, we collected the heart, liver, kidney, spleen, lungs, brain, and stomach for fluorescence analysis (Figure 5). The biodistribution is reported in percent-injected dose per gram of tissue (%ID/g), which was determined based of standard curves using homogenized organs spiked with TMV/SNP of known concentration. The biodistribution profile for each nanoparticle formulation followed the same trend: the majority of TMV, PEGylated TMV and SNPs accumulated in liver and spleen. Differences were noted in the clearance profiles: while rod-shaped TMV and PEGylated TMV was still detectable in liver and spleen 24 hours post administration, SNP formulations appeared to be cleared from tissues within one day. Data are consistent with immunofluorescence imaging of sectioned tissues (see below and supporting information).

Immunofluorescence imaging of liver- and spleen-sections

The majority of TMV and SNPs were deposited in liver and spleen; therefore we sought to analyze these tissues further and prepared cryosections for immunofluorescence analysis and colocalization studies with macrophages (F4/80 marker), B-cells (B220 marker), and T-cells (CD3 marker). Within the liver sections, Cy5-TMV, Cy5-PEG-TMV, and Cy5-SNP were found to be colocalized with macrophage marker F4/80 (Figure 6, Supporting Table 1, Supporting Figures 5-7), which is consistent with clearance of the proteinaceous nanoparticle formulations via the mononuclear phagocytotic system (MPS). Consistent with data reported by fluorescence assay, SNPs appeared to be cleared from liver macrophages faster compared to TMV rods (independent of PEGylation).

Distribution in the spleen followed a different pattern: at the 4-hour time point TMV rods and SNPs were co-localized with the marginal zone macrophages surrounding the spleen's B-cell follicles. At 24 and 96 hours post administration, the TMV and SNP signals appear to be colocalized with B-cell stain marker B220 (Figure 6, Supporting Table 1, Supporting Figures 5-7). We noticed significantly less TMV/SNP signal in B-cell follicles at 96 hours *versus* 24 hours, which is consistent with quantitative biodistribution data and may indicate

tissue clearance (loss of fluorescent signal however cannot be ruled out, see discussion). Although quantitative data (see Figure 5) indicate clearance of SNPs from the spleen by 24 hours post-administration, some signal was still apparent in confocal microscopy (Figure 6). Co-localization with T-cell marker or increased activation of T-cells was not apparent in any of our studies (Supporting Figures 8-9).

No pathological changes were noted based on histological examination of tissues

Histological examination of tissues comparing PBS and TMV/SNP-inoculated animals included livers and spleens 4, 24, 96 hours, and 14 days post-administration of TMV and SNP formulations. No pathological changes were noted. Microscopic findings were similar between TMV/SNP-inoculated and control animals, with no signs of overt toxicity and inflammation, such as tissue degeneration, apoptosis, or necrosis in any of the examined tissues (Supporting Figures 1-4).

Discussion

The shape, size, and surface properties of nanoparticles influence their *in vivo* behaviors, such as circulation half-life, biodistribution, and clearance mechanism [32-34]. Shielding strategies, such as PEGylation, of nanoparticles is often effective to increase circulation half-life by reducing opsonization and lowering mononuclear phagocyte recognition. Furthermore, recent research indicates that elongated nanomaterials with high aspect ratio (aspect ratio is defined as length divided by width) have demonstrated some beneficial *in vivo* properties for biomedical applications, such as enhanced margination properties for improved endothelial targeting [35-37], and most importantly, evasion of macrophages leading to prolonged circulation [38].

In this work, we studied biodistribution, biocompatibility, and clearance of TMV in mice. Rod-shaped TMV and spherical SNPs as well as PEGylated formulations were considered to address the following fundamental questions: first, whether nanoparticle shape impacts the *in vivo* fate of TMV and second, whether PEGylation would enhance pharmacokinetics and alter biodistribution. The data gained lay a foundation for the further development and application of TMV for biomedical applications, such as imaging and drug delivery. Overall, the data indicate clearance of TMV by liver and spleen, irrespective of shape and surface coating (i.e. PEG). Comparing spherical *versus* rod-shaped TMV, differences were noted: SNPs show shorter circulation and appear to be cleared more rapidly from tissues. The TMV-based formulations show good blood biocompatibility; further immunohistochemistry indicated that TMV does not induce adverse effects in tissues (however, more detailed organ-function assays would need to be conducted to further support this observation). Within liver and spleen TMV and SNPs localize within macrophages and B-cells, which is consistent with clearance by the RES and MPS, and may also indicate immunogenic processing of the proteinaceous nanoparticle.

Polymer coating of nanoparticles to create a stealth layer is an accepted strategy to improve circulation half-life [39]. The most popular stealth coating is polyethylene glycol (PEG) [40]. PEG provides a neutral charged hydrophilic layer that reduces opsonization by serum proteins leading to lowered recognition by MPS of the RES [41, 42]. While there are no reports comparing the pharmacokinetics of native and PEGylated VNPs; this has been demonstrated using various other nanoparticles. For example, the circulation half-life of hydrogel nanoparticles (80 nm × 80 nm × 320 nm) increased from 0.89 hours to 19.5 hours after application of a thick coating (brush morphology) of PEG_{5000} [40]. Here, we have demonstrated that TMV rods coated with a low-density PEG_{2000} layer increased the circulation half-life from 3.6 to 6.6 minutes; therefore potentially allowing a majority of the

injected particles to interact with a diseased area an additional ~30 times (~10 cycles per minute).

To assess whether TMV-based nanoparticles remain structurally sound upon intravenous administration, we assessed their stability in plasma. In brief, TMV nanorods were incubated in native and heat-inactivated plasma, collected by ultrapelleting, and analyzed by TEM imaging, which confirmed the presence of intact TMV rods (Supporting Figure 10). Considering the mild environment in blood (average salt concentration of ~ 140 mM with a pH of 7.4) it is not surprising the TMV remain structurally sound. Both TMV and SNPs withstand a range of temperature, pH, and salt conditions. Furthermore, the lack of detectable signals from the kidneys indicate that disassembly into coat proteins upon intravenous administration is unlikely (based on the low molecular weight and small size, free coat proteins would be cleared through the kidneys, while assembled high molecular weight complexes are expected to be cleared by the MPS, as observed).

While PEG-coating increased the circulation time of TMV, it should be noted that shape-derived effects were even more profound: a significantly higher dose of TMV rods remains in circulation over longer time periods compared to SNPs. At 60 minutes post i.v. administration of TMV vs. SNP, 20% ID TMV remained in circulation, while only 5% ID SNPs were detected. This is reflected by the increased phase II half-lives of 94.9 minutes for TMV and 58.2 minutes for SNPs. This phenomenon has been reported using various synthetic nanoparticle systems: for example synthetic polymeric filomicelles show enhanced circulation compared to spherical micelles made of the same polymer, and could be explained by the fact that the high aspect ratio materials are less likely taken up by MPS [43]. There is increasing supporting data showing that elongated particles avoid clearance by phagocytosis because of their larger and more complex contact angles between the nanoparticle and phagocytotic cell [29]. This has been demonstrated with gold nanoparticles where the circulation half-life of rods was significantly longer than their spherical shaped counterpart [44].

Tailoring the circulation times is critical for successful clinical application; for example, the circulation times must be carefully adjusted in imaging applications to ensure fast accumulation of the contrast agent at the target site, followed by rapid clearance. On the other hand, enhanced circulation times may be desired for tumor homing and drug delivery. Passive tumor homing is achieved making use of the enhanced permeability and retention (EPR) effect, and it is indicated that enhanced circulation of PEGylating nanoparticles increase tumor homing [43]. Indeed, it has been shown that PEGylated CPMV shows enhanced tumor homing compared to native CPMV [45]. Similarly, PEGylated bacteriophage MS2 successfully targeted breast cancer tumors, demonstrating the versatility and utility of PEGylation to cancer targeting [46]. For other diseases requiring active targeting, such as arterial inflammation, longer circulation times provide more chances for the targeted nanoparticle to interact with its target [47].

We hypothesize that pharmacokinetics of SNPs and TMV rods could be further enhanced through enhanced PEGylation, or by application of different PEG conformations. The conformation of PEG chains could either be mushroom or brush, and is determined based on the dimension of the PEG and its grafting density. The size of PEG is characterized by its Flory radius ($R_F = \alpha N^{3/5}$), where α is the length of one monomer, 0.35 nm, and *N* is the number of monomers per polymer chain. The grafting density is given by the distance (D) separating each PEG molecule [48, 49]. A low density of PEG molecules form the mushroom conformation and is roughly defined where $R_F < D$. When $R_F > D$, the brush conformation dominates. PEG in the brush conformation is more effective at shielding of nanoparticles from opsonization compared to PEG in the mushroom conformation.

Although, reports have shown that, even when in mushroom conformation, PEG will still act as an effective shield, but to a lesser degree than in the brush conformation [40, 50]. Data indicate that TMV rods were labeled with ~400 PEG_{2000} molecules per 300 nm rod (20% of coat proteins). The low loading yields a PEG density (A) of 39.8 nm^2/PEG (A=surface area of TMV/number of PEGs). From here, we can estimate the distance (D) separating each PEG molecule to be 7.1 nm ($D=2\sqrt{\frac{A}{\pi}}$). Here, PEG_{2000} has an $R_F \approx 3.5$ and therefore at this density, the PEG molecules will be in the mushroom conformation (because $R_F<D$). In order for PEG_{2000} to form the brush conformation on TMV, we would need at least 85% of the coat proteins to have PEG_{2000} molecules attached. Alternatively, higher molecular weight PEG (at least 5000) could be used; for example, only 30% coating of TMV rods is required to achieve $R_F>D$ leading to brush conformation.

VNPs are particularly interesting for biomedical applications because they are considered biocompatible, biodegradable, and nonhazardous towards humans [3]. Researchers have reported *in vivo* fate of spherical VNPs cowpea mosaic virus (CPMV) [51, 52], cowpea chlorotic mottle virus (CCMV) [53], bacteriophages Qβ [54], and MS2 [46] and filamentous potato virus X (PVX) [9]. For each system studied, RES clearance and deposition of VNPs in liver and spleen was observed, as indicated by sequestration by blood monocytes, dendritic cells and tissue macrophages. Overall, the reported biodistribution of plant viruses and bacteriophages follows a similar trend and is in agreement with the biodistribution of TMV and SNP reported here. The accumulation of nanoparticles in the liver and spleen 4 hours post injection is also consistent with the tissue distribution of other nanoparticle formulations [33].

The cryosectioning analysis indicates high colocalization of TMV particles (Cy5-TMV, PEG-Cy5-TMV, Cy5-SNP) with liver macrophages (kupffer cells) at 4 hours. This is consistent with previous reports that kupffer cells are the primary clearance mechanism for nanoparticles in circulation [55]. Data indicate that the rod-shaped particles (Cy5-TMV and PEG-Cy5-TMV) undergo hepatobiliary processing followed by excretion from the body within 24 to 96 hours. It is interesting to note that SNPs appear to follow much faster tissue clearance. SNPs were no longer detected 24 hours post administration. This is presumably due to the less stable structure of the SNPs, allowing a faster breakdown and removal from the tissue. The coat proteins of the rods are held tightly together by the single-strand RNA embedded in its structure. Formation of spheres removes the RNA and the SNPs are held together only by protein-protein interactions. The faster tissue clearance of SNPs may reduce potential toxic side effects, particularly when delivering toxic therapeutic cargos or contrast agents. Quick hepatobiliary clearance of nanoparticles is critical and remains a critical barrier to translation of nanoparticle systems. Hard inorganic nanoparticles, such as single-walled carbon nanotubes (SWNTs), gold, and silica, are secreted slowly after uptake in the liver and spleen. It can up to two months for SWNTs to be cleared from mice [56]. Other hard nanoparticles also remain in RES organs for even longer times, such as gold, which leads to unwanted toxic effects in these organs [57]. The fast clearance of the protein-based VNPs thus may offer a significant advantage over synthetic nanoparticles.

Nanoparticle toxicity is a significant concern for a variety of nanoparticles due to their long retention times [57, 58]. The toxic effects of long-term retention of nanoparticles in organs include inflammation and apoptosis. In agreement with rather fast tissue clearance, H&E-stained livers and spleens did not indicate signs of overt toxicity and inflammation, such as tissue degeneration, apoptosis, or necrosis in any of the examined tissues, thus further supporting biocompatibility of the TMV platform.

The spleen's role in the body is to act as a blood filter, removing and replacing worn out red blood cells, and it is the center of activity in the RES system. The spleen is made up of two distinct zones - red pulp and white pulp – with a marginal zone made up of antigen presenting cells bordering these areas. The red pulp contains nearly half of the body's monocytes and is where some TMV particles initially accumulate after filtration through this organ. Our results imply that a significant amount of TMV particles are filtered to the marginal zone for presentation to the lymphoid white pulp. B-cells in the white pulp then accept the TMV particles over time and presumably synthesize antibodies, since TMV is a foreign material. Localization of TMV particles with B-cell follicles is characteristic of a humoral immune response [59, 60]. Interestingly, the PEG shielding did not affect the outcome of rod-shaped TMV in the spleen. As mentioned previously, the PEG shielding on these particles is low density, meaning that a more optimized formulation may lead to better splenic avoidance and a decrease in potential immune response.

In an effort to confirm the biocompatibility of TMV particles, blood hemolysis and coagulation assays were performed. Both assays performed indicated blood biocompatibility of TMV rods and spheres. Increases or decreases in blood coagulation could lead to serious side effects such as increased cardiovascular events or bleeding out. An increase or decrease in clotting times would therefore indicate the nanoparticles activated or deactivated platelets or factors within the coagulation system. An increase or decrease in clot firmness would indicate that the particles affect primarily the interaction of the fibrinogen and platelets [61]. Previous groups have observed significant effects of particle/microbead treatments on ROTEM-measured clotting times in the range of 10-70% change from baseline controls [62, 63]. Here, there was negligible difference in the parameters studied, therefore suggesting that TMV particles do not directly interfere with the coagulation mechanism, neither do they induce cell lysis, and therefore the data further provide support indicating biocompatibility.

Viruses were discovered more than 100 years ago; in fact, TMV was the first virus to be discovered and studied. Classical *virology* has long focused on the understanding of virus structure and virus-host interactions, and advances in virology have led to significant advances in structural biology, genetics, medicine, and related disciplines. The field of *applied virology* has attracted chemists and engineers; who started to approach viruses from a different perspective and see them as platforms, as nanostructured materials providing a three-dimensional scaffold for controlled arrangement of functional molecules. This led to the design, development, and testing of virus-based materials for potential commercialization in devices (e.g., batteries and storage devices), as well as delivery vehicles for medical imaging, drug delivery, and vaccines. The field has grown out of its infancy, and the utility of virus-based materials is emerging. To realize a potential clinical application, detailed understanding of the *in vivo* properties must be gained.

It is generally understood that plant viruses are part of the food chain and found in many crops and vegetables; they are considered safe [64]. Specific to this report, TMV particles are found in nearly all cigarettes, and recently were found in the saliva of cigarette smokers [65]. Further investigation of TMV in humans revealed that antibodies against TMV are prevalent in the population [66] with smokers developing higher concentrations of these antibodies. Although reports indicate that TMV may be entering human cells, it is not replicating [67], further supporting the development of TMV as a medical cargo delivery vehicle. The application of plant viruses in the medical sector is becoming a growing field of interest and impact; therefore, more extensive investigation into the interaction of plant viruses, specifically TMV, in the body is required. Toward this goal, we provided a thorough analysis and discussion of the *in vivo* profile of rod-shaped and spherical TMV nanoparticles. Although differences were noted, all three formulations (SNP, TMV, PEG-TMV) followed a similar the overall trend regarding blood compatibility, pharmacokinetics,

biodistribution, and clearance: TMV-based materials do not induce apparent toxic effects and show fast plasma and tissue clearance profiles, desired properties for medical cargo delivery vehicles.

Conclusion

TMV rods measuring 300×18 nm were engineered to include fluorescent Cy5 dyes for imaging and injected as is (Cy5-TMV) or with a PEG coating (PEG-Cy5-TMV). We thermally transitioned Cy5-TMV rods into ~50 nm spherical particles (Cy5-SNP) to test the effect of shape without changing the surface properties (same coat protein make-up). We found that the rod-shaped particles have a longer circulation half-life compared to spheres and that PEGylation also increased the circulation half-life. Mononuclear phagocytes in RES organs, i.e. the liver and the spleen, clear each particle formulation. The plasma clearance and tissue response is typical for protein-based nanoparticles, and nanoparticle in general. Future studies set out to investigate the immune response further; as TMV and SNPs were found to be co-localized with B-cells indicating activation of the immune response. Overall TMV rods and spheres follow typical biodistribution and fast tissue clearance, the latter is important and provides an advantage over synthetic nanoparticle formulations, which may persist in cells and tissues over long time periods. Our data indicate blood and tissue biocompatibility, as toxic effects were not apparent. Giving the data reported here, in combination with the particle properties, high aspect ratio, multivalency, TMV fulfills various requirements according to emerging design rules that are being explored in nanomedical engineering [68]. This work sets the stage for further engineering and application of TMV in the health care sector.

Supplementary Material

Refer to Web version on PubMed Central for supplementary material.

Acknowledgments

This work was supported by NIH P30 EB011317 grant, Mt. Sinai Foundation, and NIH T32 HL105338 training grant. Dr. Marianne Manchester (UCSD) and Dr. Jack Johnson (TSRI) are thanked for helpful discussion.

References

[1]. Parveen S, Misra R, Sahoo SK. Nanoparticles: a boon to drug delivery, therapeutics, diagnostics and imaging. Nanomedicine: Nanotechnology, Biology, and Medicine. 2012; 8:147–66.

[2]. Zhu M, Nie G, Meng H, Xia T, Nel A, Zhao Y. Physicochemical Properties Determine Nanomaterial Cellular Uptake, Transport, and Fate. Acc Chem Res. 2012

[3]. Yildiz I, Shukla S, Steinmetz NF. Applications of viral nanoparticles in medicine. Current Opinion in Biotechnology. 2011; 22:901–8. [PubMed: 21592772]

[4]. Steinmetz NF, Ablack AL, Hickey JL, Ablack J, Manocha B, Mymryk JS, Luyt LG, Lewis JD. Intravital Imaging of Human Prostate Cancer Using Viral Nanoparticles Targeted to Gastrin-Releasing Peptide Receptors. Small. 2011; 7:1664–72. [PubMed: 21520408]

[5]. Plummer EM, Thomas D, Destito G, Shriver LP, Manchester M. Interaction of cowpea mosaic virus nanoparticles with surface vimentin and inflammatory cells in atherosclerotic lesions. Nanomedicine. 2012

[6]. Brunel FM, Lewis JD, Destito G, Steinmetz NF, Manchester M, Stuhlmann H, Dawson PE. Hydrazone ligation strategy to assemble multifunctional viral nanoparticles for cell imaging and tumor targeting. Nano Letters. 2010; 10:1093–7. [PubMed: 20163184]

[7]. Wu Z, Chen K, Yildiz I, Dirksen A, Fischer R, Dawson PE, Steinmetz NF. Development of viral nanoparticles for efficient intracellular delivery. Nanoscale. 2012; 4:3567–76. [PubMed: 22508503]

[8]. Gandra N, Abbineni G, Qu X, Huai Y, Wang L, Mao C. Bacteriophage Bionanowire as a Carrier for Both Cancer-Targeting Peptides and Photosensitizers and its use in Selective Cancer Cell Killing by Photodynamic Therapy. Small. 2012; 9:215–21. [PubMed: 23047655]

[9]. Shukla S, Wen AM, Ayat NR, Commandeur U, Gopalkrishnan R, Broome AM, Lozada KW, Keri RA, Steinmetz NF. Biodistribution and clearance of a filamentous plant virus in healthy and tumorbearing mice. Nanomedicine. 2013

[10]. Lee KL, Hubbard LC, Hern S, Yildiz I, Gratzl M, Steinmetz NF. Shape matters: the diffusion rates of TMV rods and CPMV icosahedrons in a spheroid model of extracellular matrix are distinct. Biomaterials Science. 2013; 1:581–8.

[11]. Shukla S, Ablack AL, Wen AM, Lee KL, Lewis JD, Steinmetz NF. Increased Tumor Homing and Tissue Penetration of the Filamentous Plant Viral Nanoparticle Potato virus X. Molecular Pharmaceutics. 2013; 10:33–42. [PubMed: 22731633]

[12]. Klug A. The tobacco mosaic virus particle: structure and assembly. Philos Trans R Soc Lond B Biol Sci. 1999; 354:531–5. [PubMed: 10212932]

[13]. Soto CM, Ratna BR. Virus hybrids as nanomaterials for biotechnology. Current Opinion in Biotechnology. 2010; 21:426–38. [PubMed: 20688511]

[14]. Liu Z, Qiao J, Niu Z, Wang Q. Natural supramolecular building blocks: from virus coat proteins to viral nanoparticles. Chem Soc Rev. 2012; 41:6178–94. [PubMed: 22880206]

[15]. Miller RA, Presley AD, Francis MB. Self-assembling light-harvesting systems from synthetically modified tobacco mosaic virus coat proteins. Journal of the American Chemical Society. 2007; 129:3104–9. [PubMed: 17319656]

[16]. Miller RA, Stephanopoulos N, McFarland JM, Rosko AS, Geissler PL, Francis MB. Impact of Assembly State on the Defect Tolerance of TMV-Based Light Harvesting Arrays. Journal of the American Chemical Society. 2010; 132:6068–74. [PubMed: 20392093]

[17]. Chen X, Gerasopoulos K, Guo J, Brown A, Wang C, Ghodssi R, Culver JN. Virus-enabled silicon anode for lithium-ion batteries. ACS Nano. 2010; 4:5366–72. [PubMed: 20707328]

[18]. Bruckman MA, Liu J, Koley G, Li Y, Benicewicz B, Niu Z, Wang Q. Tobacco mosaic virus based thin film sensor for detection of volatile organic compounds. Journal of Materials Chemistry. 2010; 20:5715.

[19]. Kaur G, Valarmathi MT, Potts JD, Jabbari E, Sabo-Attwood T, Wang Q. Regulation of osteogenic differentiation of rat bone marrow stromal cells on 2D nanorod substrates. Biomaterials. 2010; 31:1732–41. [PubMed: 20022632]

[20]. Bruckman MA, Kaur G, Lee LA, Xie F, Sepulveda J, Breitenkamp R, Zhang X, Joralemon M, Russell TP, Emrick T, Wang Q. Surface Modification of Tobacco Mosaic Virus with “Click” Chemistry. ChemBioChem. 2008; 9:519–23. [PubMed: 18213566]

[21]. Bruckman MA, Hern S, Jiang K, Flask CA, Yu X, Steinmetz NF. Tobacco mosaic virus rods and spheres as supramolecular high-relaxivity MRI contrast agents. J Mater Chem B. 2013; 1:1482–90.

[22]. Koo M, Bendahmane M, Lettieri GA, Paoletti AD, Lane TE, Fitchen JH, Buchmeier MJ, Beachy RN. Protective immunity against murine hepatitis virus (MHV) induced by intranasal or subcutaneous administration of hybrids of tobacco mosaic virus that carries an MHV epitope. Proceedings of the National Academy of Sciences of the United States of America. 1999; 96:7774–9. [PubMed: 10393897]

[23]. Fitchen J, Beachy RN, Hein MB. Plant virus expressing hybrid coat protein with added murine epitope elicits autoantibody response. Vaccine. 1995; 13:1051–7. [PubMed: 7491811]

[24]. McCormick AA, Corbo TA, Wykoff-Clary S, Palmer KE, Pogue GP. Chemical conjugate TMV-peptide bivalent fusion vaccines improve cellular immunity and tumor protection. Bioconjugate Chem. 2006; 17:1330–8.

[25]. McCormick AA, Corbo TA, Wykoff-Clary S, Nguyen LV, Smith ML, Palmer KE, Pogue GP. TMV-peptide fusion vaccines induce cell-mediated immune responses and tumor protection in two murine models. Vaccine. 2006; 24:6414–23. [PubMed: 16860441]

[26]. Atabekov J, Nikitin N, Arkhipenko M, Chirkov S, Karpova O. Thermal transition of native tobacco mosaic virus and RNA-free viral proteins into spherical nanoparticles. Journal of General Virology. 2011; 92:453–6. [PubMed: 20980527]

[27]. Nikitin NA, Malinin AS, Rakhnyanskaya AA, Trifonova EA, Karpova OV, Yaroslavov AA, Atabekov JG. Use of a polycation spacer for noncovalent immobilization of albumin on thermally modified virus particles. Polymer Science Series A. 2011; 53:1026–31.

[28]. Karpova O, Nikitin N, Chirkov S, Trifonova E, Sheveleva A, Lazareva E, Atabekov J. Immunogenic compositions assembled from TMV-generated spherical particle platforms and foreign antigens. Journal of General Virology. 2011

[29]. Albanese A, Tang PS, Chan WCW. The Effect of Nanoparticle Size, Shape, and Surface Chemistry on Biological Systems. Annual Review of Biomedical Engineering. 2012; 14:1–16.

[30]. Leberman R. The isolation of plant viruses by means of “simple” coacervates. Virology. 1966; 30:341–7. [PubMed: 5921640]

[31]. Siller-Matula JM, Plasenzotti R, Spiel A, Quehenberger P, Jilma B. Interspecies differences in coagulation profile. Thrombosis and haemostasis. 2008; 100:397–404. [PubMed: 18766254]

[32]. Sa LTM, de Souza Albernaz M, de Carvalho Patricio BF, Junior MVF, Coelho BF, Bordim A, Almeida JC, Santos-Oliveira R. Biodistribution of nanoparticles: Initial considerations. Journal of Pharmaceutical and Biomedical Analysis. 2012; 70:602–4. [PubMed: 22742922]

[33]. Li S-D, Huang L. Pharmacokinetics and Biodistribution of Nanoparticles. Mol Parmaceutics. 2008; 5:496–504.

[34]. Longmire MR, Ogawa M, Choyke PL, Kobayashi H. Biologically optimized nanosized molecules and particles: more than just size. Bioconjugate Chem. 2011; 22:993–1000.

[35]. Lee S-Y, Ferrari M, Decuzzi P. Design of bio-mimetic particles with enhanced vascular interaction. Journal of Biomechanics. 2009; 42:1885–90. [PubMed: 19523635]

[36]. Gentile F, Chiappini C, Fine D, Bhavane RC, Peluccio MS, Cheng MM-C, Liu X, Ferrari M, Decuzzi P. The effect of shape on the margination dynamics of non-neutrally buoyant particles in twodimensional shear flows. Journal of Biomechanics. 2008; 41:2312–8. [PubMed: 18571181]

[37]. Decuzzi P, Ferrari M. The adhesive strength of non-spherical particles mediated by specific interactions. Biomaterials. 2006; 27:5307–14. [PubMed: 16797691]

[38]. Decuzzi P, Godin B, Tanaka T, Lee SY, Chiappini C, Liu X, Ferrari M. Size and shape effects in the biodistribution of intravascularly injected particles. Journal of Controlled Release. 2010; 141:320–7. [PubMed: 19874859]

[39]. Storm G, Belliot SO, Daemen T, Lasic DD. Surface modification of nanoparticles to oppose uptake by the mononuclear phagocyte system. Adv Drug Deliver Rev. 1995; 17:31–48.

[40]. Perry JL, Reuter KG, Kai MP, Herlihy KP, Jones SW, Luft JC, Napier M, Bear JE, DeSimone JM. PEGylated PRINT Nanoparticles: The Impact of PEG Density on Protein Binding, Macrophage Association, Biodistribution, and Pharmacokinetics. Nano Lett. 2012 120905163100009.

[41]. Owens DE 3rd, Peppas NA. Opsonization, biodistribution, and pharmacokinetics of polymeric nanoparticles. Int J Pharm. 2006; 307:93–102. [PubMed: 16303268]

[42]. Knop K, Hoogenboom R, Fischer D, Schubert US. Poly(ethylene glycol) in Drug Delivery: Pros and Cons as Well as Potential Alternatives. Angew Chem Int Edit. 2010; 49:6288–308.

[43]. Geng Y, Dalhaimer P, Cai SS, Tsai R, Tewari M, Minko T, Discher DE. Shape effects of filaments versus spherical particles in flow and drug delivery. Nature Nanotechnology. 2007; 2:249–55.

[44]. Arnida, Janát-Amsbury MM, Ray A, Peterson CM, Ghandehari H. Geometry and surface characteristics of gold nanoparticles influence their biodistribution and uptake by macrophages. Eur J Pharm Biopharm. 2011; 77:417–23. [PubMed: 21093587]

[45]. Steinmetz NF. Viral nanoparticles as platforms for next-generation therapeutics and imaging devices. Nanomedicine. 2010; 6:634–41. [PubMed: 20433947]

[46]. Farkas ME, Aanei IL, Behrens CR, Tong GJ, Murphy ST, O’Neil JP, Francis MB. PET Imaging and biodistribution of chemically modified bacteriophage MS2. Mol Parmaceutics. 2013; 10:69–76.

[47]. Sen Gupta A. Nanomedicine approaches in vascular disease: a review. Nanomedicine: Nanotechnology, Biology, and Medicine. 2011; 7:763–79.

[48]. De Gennes PG. Polymers at an interface; a simplified view. Advances in Colloid and Interface Science. 1987; 27:189–209.

[49]. Wattendorf U, Merkle HP. PEGylation as a tool for the biomedical engineering of surface modified microparticles. J Pharm Sci. 2008; 97:4655–69. [PubMed: 18306270]

[50]. Steinmetz NF, Manchester M. PEGylated viral nanoparticles for biomedicine: the impact of PEG chain length on VNP cell interactions in vitro and ex vivo. Biomacromolecules. 2009; 10:784–92. [PubMed: 19281149]

[51]. Rae CS, Wei Khor I, Wang Q, Destito G, Gonzalez MJ, Singh P, Thomas DM, Estrada MN, Powell E, Finn MG, Manchester M. Systemic trafficking of plant virus nanoparticles in mice via the oral route. Virology. 2005; 343:224–35. [PubMed: 16185741]

[52]. Singh P, Prasuhn D, Yeh RM, Destito G, Rae CS, Osborn K, Finn MG, Manchester M. Biodistribution, toxicity and pathology of cowpea mosaic virus nanoparticles in vivo. J Control Release. 2007; 120:41–50. [PubMed: 17512998]

[53]. Kaiser CR, Flenniken ML, Gillitzer E, Harmsen AL, Harmsen AG, Jutila MA, Douglas T, Young MJ. Biodistribution studies of protein cage nanoparticles demonstrate broad tissue distribution and rapid clearance in vivo. International Journal of Nanomedicine. 2007; 2:715–33. [PubMed: 18203438]

[54]. Prasuhn DE Jr. Singh P, Strable E, Brown S, Manchester M, Finn MG. Plasma clearance of bacteriophage Qbeta particles as a function of surface charge. Journal of the American Chemical Society. 2008; 130:1328–34. [PubMed: 18177041]

[55]. Sadauskas E, Wallin H, Stoltenberg M, Vogel U, Doering P, Larsen A, Danscher G. Kupffer cells are central in the removal of nanoparticles from the organism. Part Fibre Toxicol. 2007; 4:10. [PubMed: 17949501]

[56]. Liu Z, Davis C, Cai W, He L, Chen X, Dai H. Circulation and long-term fate of functionlized, biocompatible single-walled carbon nanotubes in mice by Raman spectroscopy. Proceedings of the National Academy of Sciences. 2008; 105:1410–5.

[57]. Gad SC, Sharp KL, Montgomery C, Payne JD, Goodrich GP. Evaluation of the Toxicity of Intravenous Delivery of Auroshell Particles (Gold-Silica Nanoshells). International Journal of Toxicology. 2013; 31:584–94. [PubMed: 23212452]

[58]. Khlebtsov N, Dykman L. Biodistribution and toxicity of engineered gold nanoparticles: a review of in vitro and in vivo studies. Chem Soc Rev. 2011; 40:1647. [PubMed: 21082078]

[59]. Murakami T, Chen X, Hase K, Sakamoto A, Nishigaki C, Ohno H. Splenic CD19 CD35+B220+ cells function as an inducer of follicular dendritic cell network formation. Blood. 2007; 110:1215–24. [PubMed: 17519390]

[60]. Bachmann MF. The role of germinal centers for antiviral B cell responses. Immunol Res. 1998; 17:329–44. [PubMed: 9638476]

[61]. Siller-Matula JM, Plasenzotti R, Spiel A, Quehenberger P, Jilma B. Interspecies differences in coagulation profile. Thromb Haemost. 2008; 100:397–404. [PubMed: 18766254]

[62]. Shoffstall AJ, Everhart LM, Varley ME, Soehnlen ES, Shick AM, Ustin JS, Lavik EB. Tuning Ligand Density on Intravenous Hemostatic Nanoparticles Dramatically Increases Survival Following Blunt Trauma. Biomacromolecules. 2013

[63]. Zipperle J, Schlimp CJ, Holnthoner W, Husa AM, Nurnberger S, Redl H, Schochl H. A novel coagulation assay incorporating adherent endothelial cells in thromboelastometry. Thromb Haemost. 2013; 109:869–77. [PubMed: 23494019]

[64]. Colson P, Richet H, Desnues C, Balique F, Moal V, Grob JJ, Berbis P, Lecoq H, Harle JR, Berland Y, Raoult D. Pepper mild mottle virus, a plant virus associated with specific immune responses, Fever, abdominal pains, and pruritus in humans. PLoS One. 2010; 5:e10041. [PubMed: 20386604]

[65]. Balique F, Colson P, Raoult D. Tobacco mosaic virus in cigarettes and saliva of smokers. J Clin Virol. 2012; 55:374–6. [PubMed: 22959216]

[66]. Liu R, Vaishnav RA, Roberts AM, Friedland RP. Humans have antibodies against a plant virus: evidence from tobacco mosaic virus. PLoS One. 2013; 8:e60621. [PubMed: 23573274]

[67]. Balique F, Colson P, Barry AO, Nappez C, Ferretti A, Moussawi KA, Ngounga T, Lepidi H, Ghigo E, Mege JL, Lecoq H, Raoult D. Tobacco mosaic virus in the lungs of mice following intra-tracheal inoculation. PLoS One. 2013; 8:e54993. [PubMed: 23383021]

[68]. Wen AM, Rambhia PH, French RH, Steinmetz NF. Design rules for nanomedical engineering: from physical virology to the applications of virus-based materials in medicine. Journal of biological physics. 2013

- TMV particles exhiit two---phase decay pharmacokinetics, with rods circulating longer than spheres.
- TMV particles arecleared from circulation by the reticuloendothelial system
- TMV particles are cleared from the liver and spleen within days
- TMV particles show blood biocompatibility and no apparent changes in tissue histology

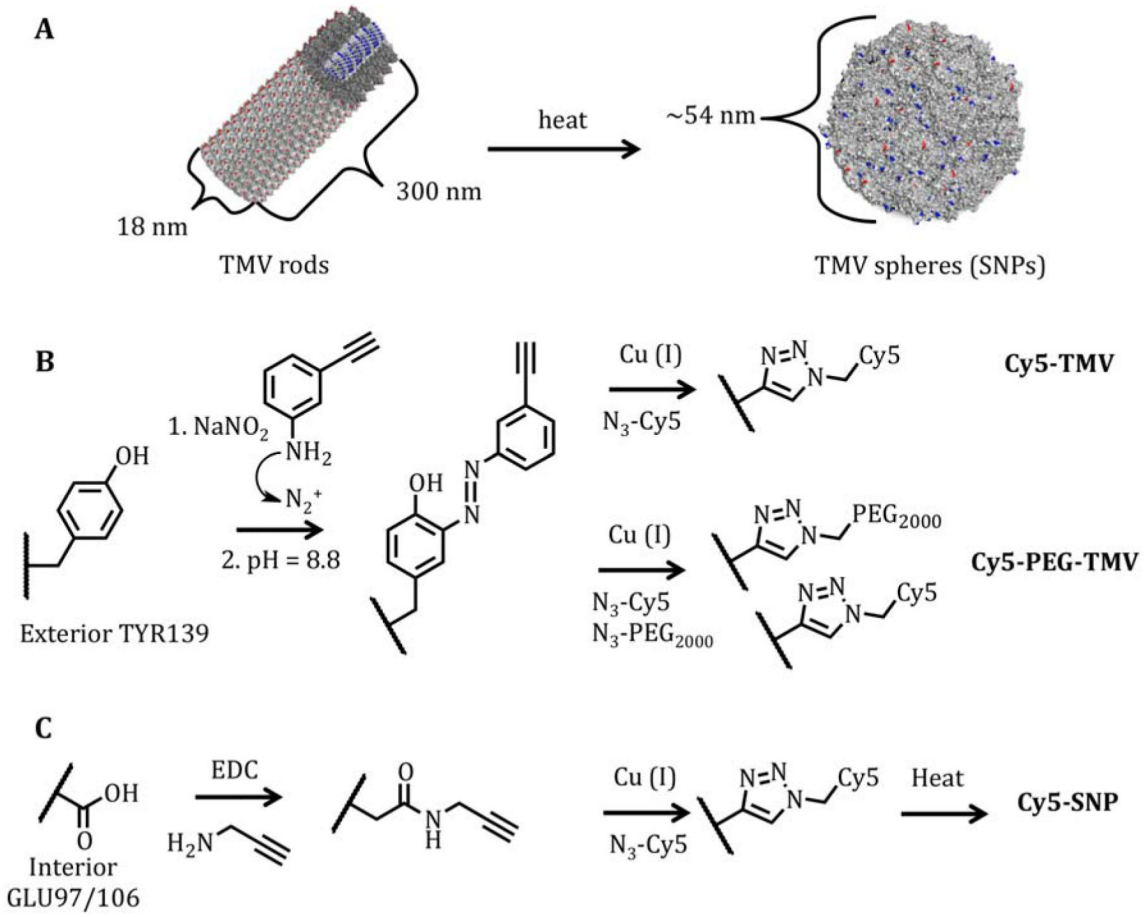

Figure 1.

(A) A PyMol generated schematic representation of the thermal transition of tobacco mosaic virus (TMV) rods to spherical nanoparticles (SNPs). Several coat proteins have been removed from the TMV rod to highlight the hollow interior with interior glutamic acids, GLU97 and GLU106, in blue and exterior tyrosine, TYR139, in red. (B) Schematic illustration of the bioconjugation reactions used to incorporate sulfo-Cy5 dyes and PEG_{2000} molecules on the exterior of TMV rods. (C) Schematic illustration showing the method to generate sulfo-Cy5 labeled SNPs.

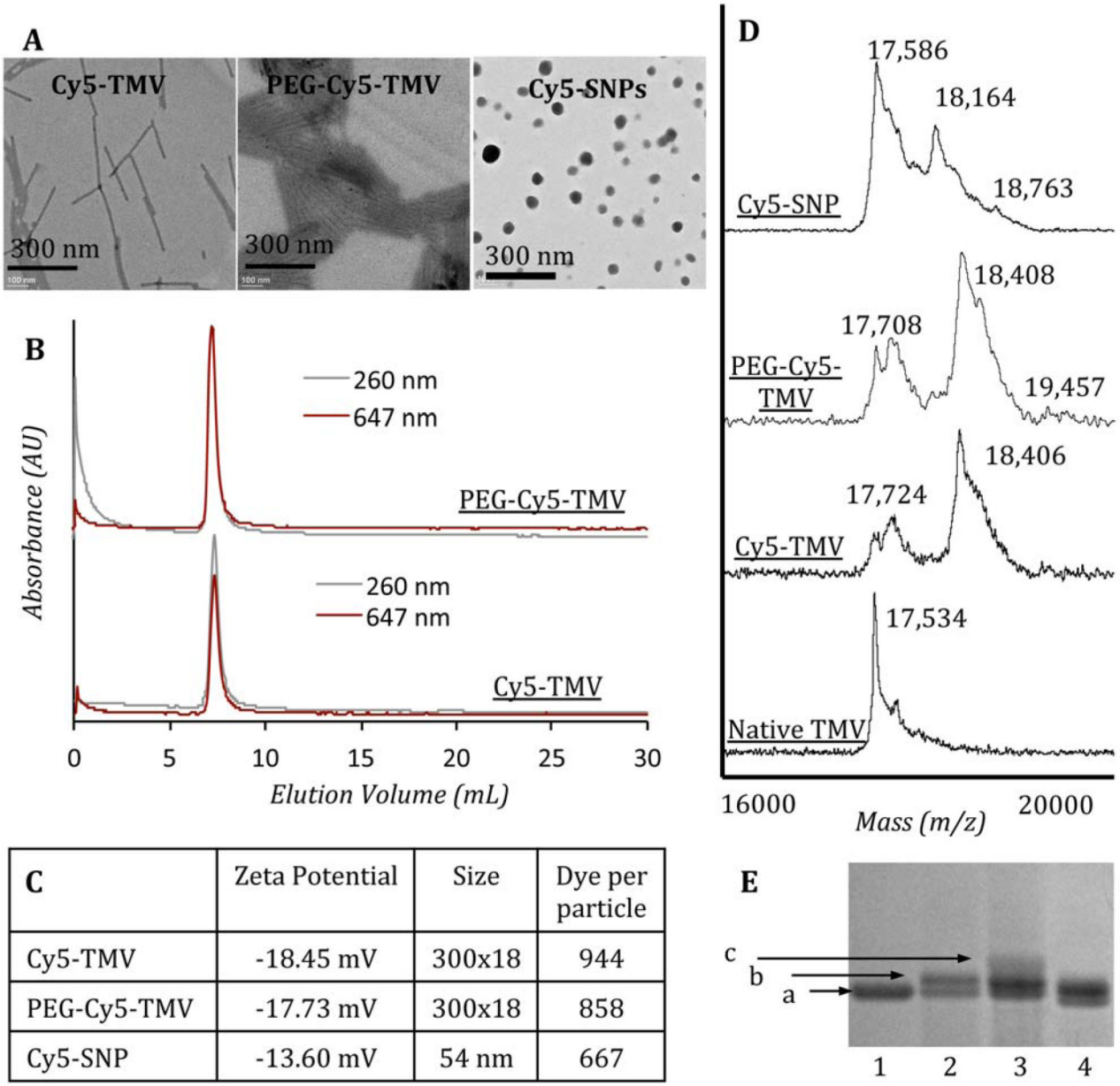

C	Zeta Potential	Size	Dye per particle
Cy5-TMV	-18.45 mV	300x18	944
PEG-Cy5-TMV	-17.73 mV	300x18	858
Cy5-SNP	-13.60 mV	54 nm	667

Figure 2.

Characterization of Cy5-TMV, PEG-Cy5-TMV, and Cy5-SNPs. (A) Transmission electron micrograph images of TMV rods and SNPs. (B) Size exclusion chromatographs of PEG-Cy5-TMV and Cy5-TMV. (C) A table comparing the charge, size and number of Cy5 dyes per particle. (D) MALDI-TOF MS spectra of native-TMV, Cy5-TMV, PEG-Cy5-TMV, and Cy5-SNP. (E) SDS-PAGE of (lane 1) native-TMV, (lane 2) Cy5-TMV, (lane 3) PEG-Cy5-TMV, and (lane 4) Cy5-SNP. The (a) unmodified ~ 18 kDa TMV coat protein, (b) Cy5 modified ~ 19 kDa coat protein, and (c) PEG modified ~ 20 kDa coat proteins are identified for reference (it should be noted that only a ratio of the coat proteins were modified, see discussion in the manuscript text).

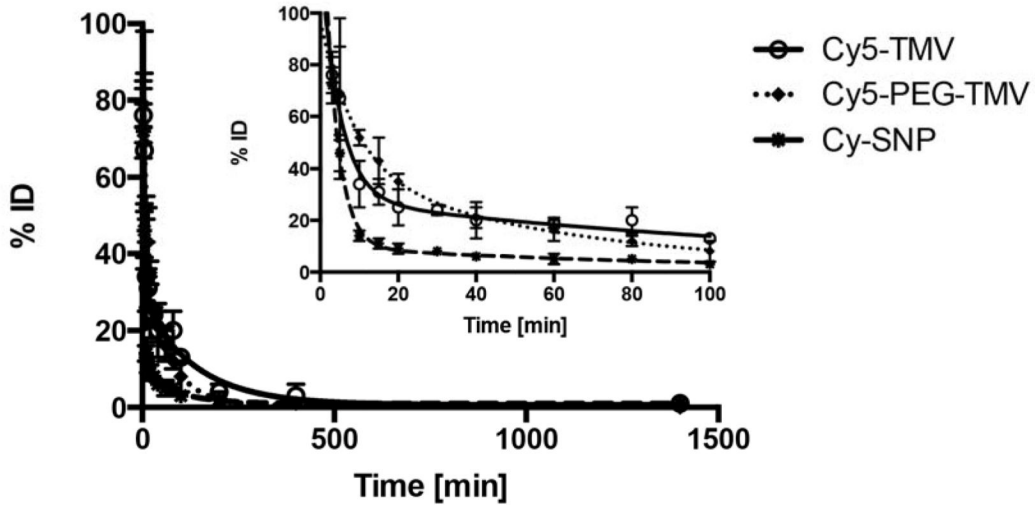

Figure 3.

Pharmacokinetics of Cy5-TMV, PEG-Cy5-TMV, and Cy5-SNP. At least three data points were collected for each time point and formulation; averages and standard deviations are shown. Data were analyzed using Prism software, and data are reported as percentage injected dose against time.

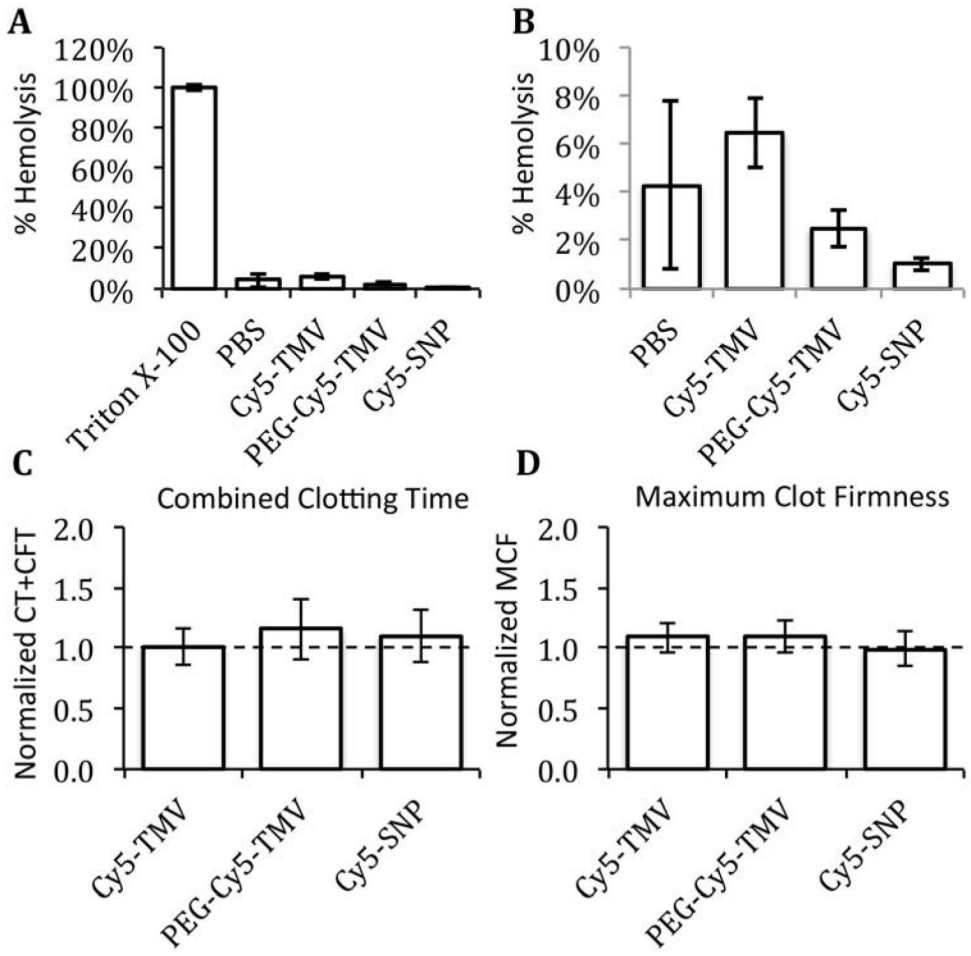

Figure 4.

Blood biocompatibility assays. (A) Red blood cell (RBC) hemolysis assay. (B) Zoomed in RBC hemolysis assay showing Cy5-TMV, PEG-Cy5-TMV, and Cy5-SNP do not lyse RBCs. (C) Effect of Cy5-TMV, PEG-Cy5-TMV, and Cy5-SNP on clotting (normalized to saline control), measured in rotational thromboelastometry (ROTEM). There were no significant changes in the combined clotting time (CT+CFT) and maximum clot firmness (MCF) compared to the saline control (dotted line). Error bars represent S.D.

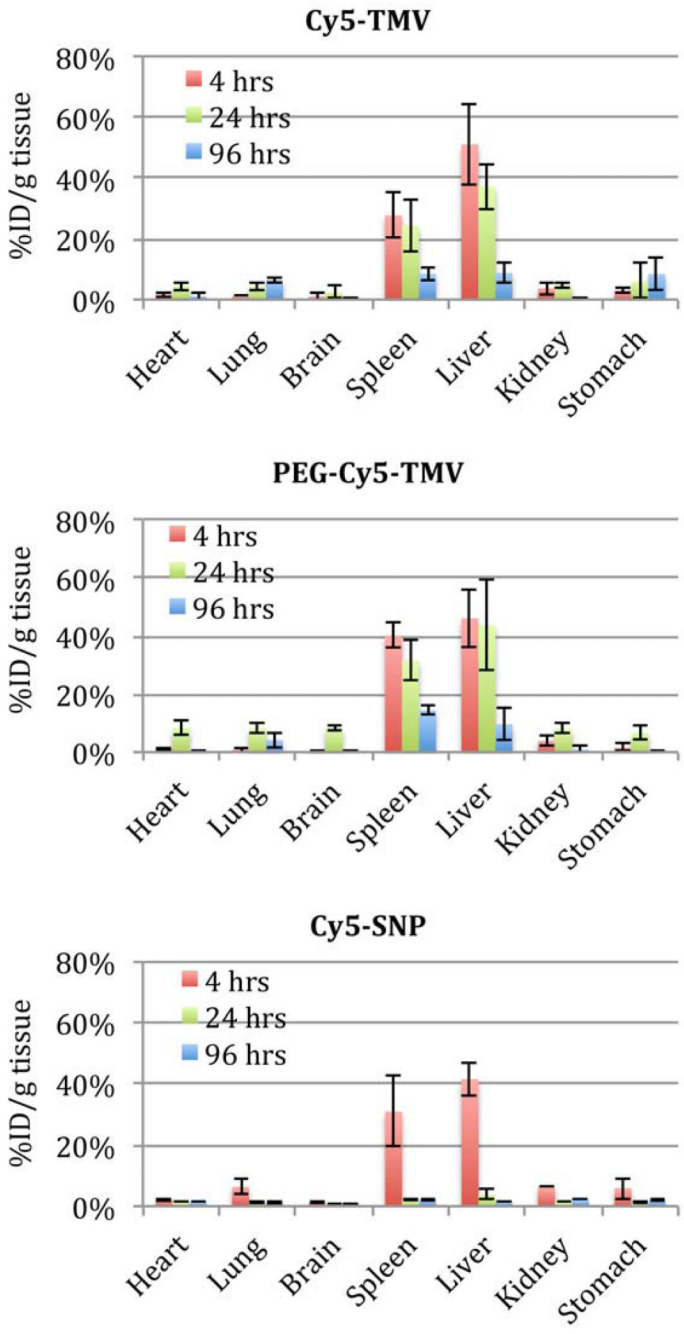

Figure 5.
Tissue biodistribution of (A) Cy5-TMV, (B) PEG-Cy5-TMV, and (C) Cy5-SNP at 4, 24, and 96 hours after I.V. injection. Three female Balb/c animals were analyzed per time point and formulations. Averages and standard deviations are shown.

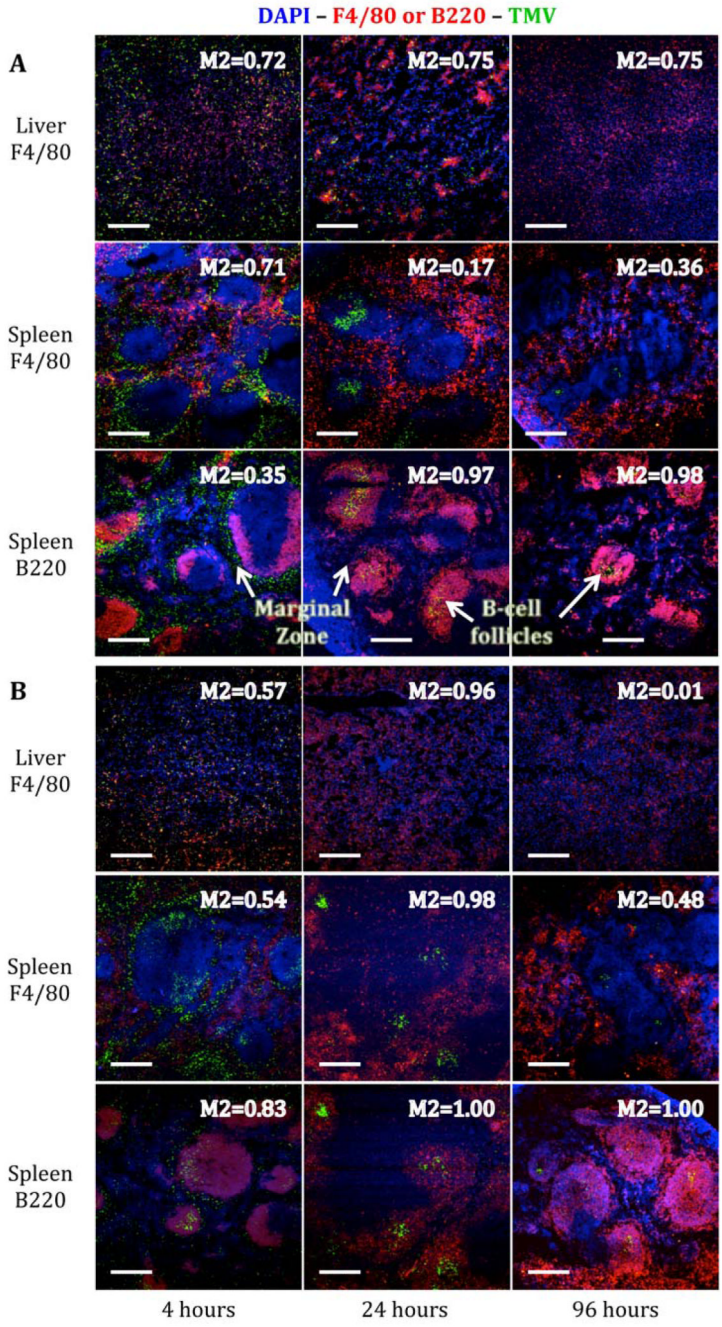

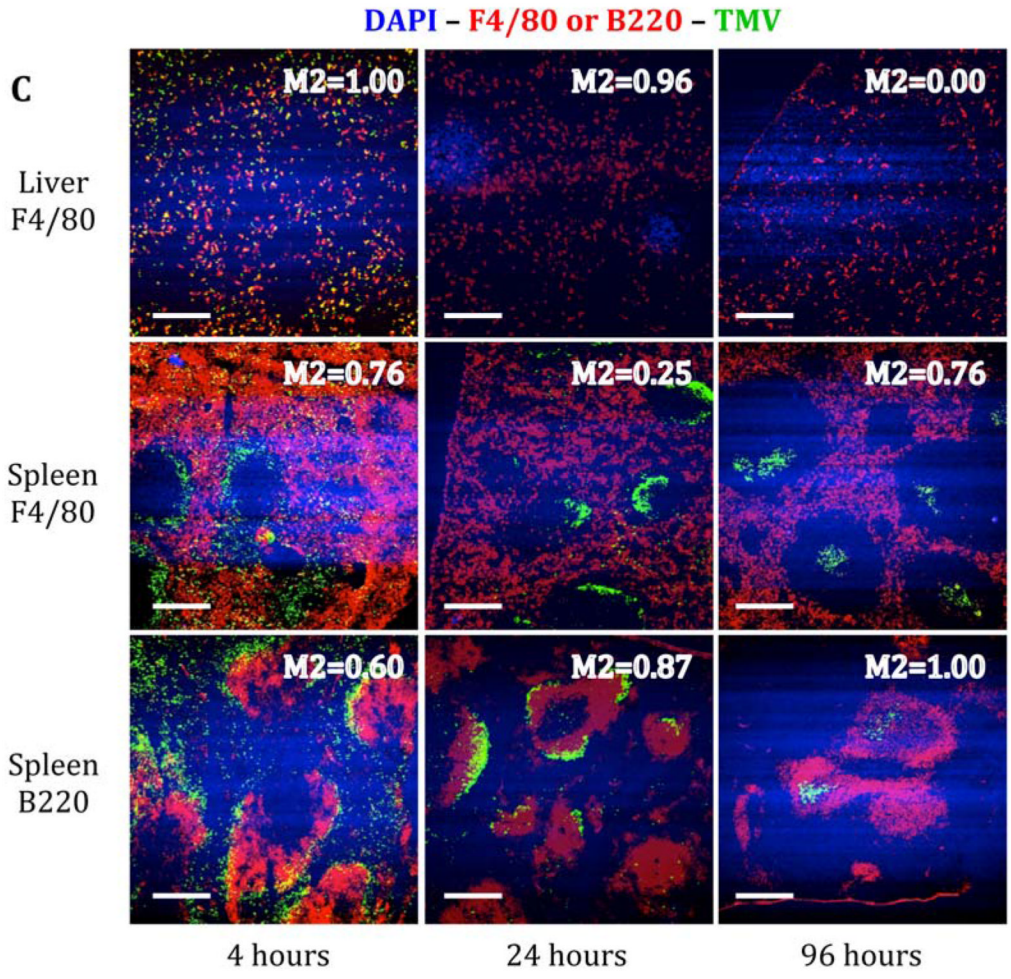

Figure 6.

Immunofluorescence imaging of liver and spleen sections 4, 24, and 96 hours after i.v. administration of (A) Cy5-TMV, (B) PEG-Cy5-TMV, and (C) Cy5-SNP (colored green). Liver sections were stained for macrophages marker F4/80 (red). Spleen sections were stained for B-cell marker B220 (red) and macrophage marker F4/80 (red). The marginal zone,and Bcell follicles are highlighted in the spleen sections (in A) for reference. Cell nuclei are stained with DAPI (blue). Inset into each image is the Manders' M2 colocalization coefficient (M2=1.0 is attributed to 100% colocalization) Data were analyzed using ImageJ software. Scale bars = 250 μm.